Obrabotka metallov (tekhnologiya, oborudovanie, instrumenty) = Metal Working and Material Science. 2026 vol. 28 no. 2 pp. 49–71
ISSN: 1994-6309 (print) / 2541-819X (online)
DOI: 10.17212/1994-6309-2026-28.2-49-71

NSTU NETI

Obrabotka metallov - Metal Working and Material Science

Journal homepage: http://journals.nstu.ru/obrabotka_metallov

Evaluation of the penetrating ability of oxide fluxes in welding carbon and low-alloy steels using novel A-TIG methods

Antonina Karlina [1, 2, a, *], *Vitaliy Gladkikh* [1, b], *Georgiy Kurdyumov* [2, c], *Roman Kononenko* [3, d], *Viktor Kondratiev* [2, 4, e]

[1] National Research Moscow State University of Civil Engineering, 26 Yaroslavskoe Shosse, Moscow, 129337, Russian Federation
[2] Cherepovets State University, 5 Lunacharsky pr., Cherepovets, 162600, Russian Federation
[3] Irkutsk National Research Technical University, 83 Lermontova str., Irkutsk, 664074, Russian Federation
[4] A.P. Vinogradov Institute of Geochemistry SB RAS, 1A Favorskiy St., Irkutsk, 664033, Russian Federation

[a] https://orcid.org/0000-0003-3287-3298, karlinat@mail.com; [b] https://orcid.org/0000-0003-1953-1584, gladkich_87@mail.ru;
[c] https://orcid.org/0009-0000-8373-1412, gekurdiumov@chsu.ru; [d] https://orcid.org/0009-0001-5900-065X, istu_politeh@mail.ru;
[e] https://orcid.org/0000-0002-7437-2291, imz@mail.ru

ARTICLE INFO

Article history:
Received: 18 January 2026
Revised: 14 March 2026
Accepted: 21 March 2026
Available online: 15 June 2026

Keywords:
Welding
Activating fluxes
Penetration depth
Coating thickness

ABSTRACT

Introduction. The purpose of this study is to evaluate the technological potential of using oxide activating fluxes in the novel *FB-TIG* and *FZ-TIG* methods to improve penetration efficiency and weld quality in carbon and low-alloy steels. This paper attempts to analyze and review the published literature concerning various hypotheses that explain the high penetration achieved using activating fluxes. **Materials and Methods.** Low-alloy steel samples with thicknesses ranging from 3 to 10 mm were used in this study. Fine flux powders were pre-dispersed in acetone. The flux was carefully applied with a brush to the upper surface of the plate over half of its length. The other half of the plate was left without flux to perform conventional *TIG* welding for comparison. Bead-on-plate welds were made without the addition of any filler material. Several parallel weld passes were deposited with sufficient spacing to avoid thermal interference. The arc current was varied in the range of 80–250 A, while the welding speed was kept constant at 100 mm/min. The welding voltage was set to 15–16 V. Heat input was calculated using the standard expression, assuming a heat transfer efficiency of 0.8. High-purity, industrial-grade argon was used as the shielding gas at a flow rate of 20 L/min. A standard optical microscope was used for metallographic examination, and a camera was used to record the welding process. **Results and Discussion.** The studies have shown that penetration depth primarily depends on such welding parameters as arc length (mm), welding current (A), and travel speed (mm/s). The depth-to-width (*D*/*W*) ratio is high for the *FB-TIG* method; moreover, surface appearance and slag detachability are improved. The influence of the acidic or alkaline nature of the flux on weld geometry and surface appearance is analyzed. Acid fluxes provide a smoother weld surface than alkaline oxide fluxes. Welding with activated *FB-TIG* and *FZ-TIG* using SiO_2 flux increases the penetration depth and the depth-to-width ratio by factors of 1.5–1.7, respectively, compared to conventional *A-TIG* welding.

For citation: Karlina A.I., Gladkikh V., Kurdyumov G., Kononenko R.V., Kondratiev V.V. Evaluation of the penetrating ability of oxide fluxes in welding carbon and low-alloy steels using novel A-TIG methods. *Obrabotka metallov (tekhnologiya, oborudovanie, instrumenty) = Metal Working and Material Science,* 2026, vol. 28, no. 2, pp. 49–71. DOI: 10.17212/1994-6309-2026-28.2-49-71. (In Russian).

Introduction

Currently, arc welding has many variants. The most widely considered processes in the plasma science literature are:

– Tungsten inert gas welding (*TIG*) – also known as gas tungsten arc welding (*GTAW*);

– Metal inert gas (*MIG*) and metal active gas (*MAG*) welding – both also referred to as gas metal arc welding (*GMAW*).

*** Corresponding author**
Karlina Antonina I., Ph.D. (Engineering), Research Associate
National Research Moscow State Construction University,
26 Yaroslavskoe shosse,
129337, Moscow, Russian Federation
Tel: +7 950 120-19-50, **e-mail:** karlinat@mail.ru

In *TIG* welding, the electrode is usually the cathode, which is a tungsten cylinder sharpened to a conical tip. Tungsten is typically doped with a rare earth element (e.g., thorium or lanthanum) to reduce the work function, thereby lowering the temperature at which thermionic electron emission can occur. *TIG* welding has been extensively studied by plasma researchers because it is a relatively simple process. As noted above, cooling the workpiece with water makes it possible to obtain a free-burning arc that is stable for tens of minutes (limited only by gradual erosion of the electrode tip) with minor contamination by metal vapors, which simplifies both measurements and modeling. Standard shielding gases include argon, helium, and their mixtures; sometimes small amounts of hydrogen are added.

With the development of industry, the requirements for welding efficiency are increasing. However, in traditional *GTAW* and *GMAW*, there is a conflict between high deposition efficiency and low thermal impact on the base metal, which limits overall process efficiency. The development of new and highly efficient welding processes has become an urgent area of research. *TIG* welding is known for its stability and ability to produce high-quality welds [1, 2].

In *TIG* welding, a free-burning arc is used as a heat source. The arc energy is not concentrated [3–5], and penetration is low [5–15]. Complete penetration is achieved only in thin plates [5–7]. The welding efficiency for thick plates is low. In addition, the current-carrying capacity of tungsten electrodes is limited [5, 6]. At high currents, erosion or even damage occurs; this shortens the service life of the welding torch and affects the quality of the weld [4–6]. Therefore, improving the penetration capability of the TIG welding process is of great importance [5–15].

For example, narrowing the arc column to increase energy density is an effective method of increasing welding efficiency [1–6]. In plasma arc welding (*PAW*), a small-diameter water-cooled nozzle is added to the torch head [16]. The arc is transformed into a strongly constricted arc under the combined influence of mechanical constriction [17], thermal constriction [18], and electromagnetic constriction [14, 15]. During the welding process, the “keyhole” effect is easily formed, and the welding efficiency is significantly increased [10–15].

The *GF-PAW* process was proposed in [19]; a focusing gas with a small flow rate is added between the plasma gas and the shielding gas of the *PAW* torch to create an additional gas constriction effect on the plasma arc. The diameter of the arc decreases, and the penetration increases. However, the focusing gas has a very limited adjustment range for ensuring plasma arc stability due to the narrow channel, and it virtually does not increase the arc pressure.

To constrict the *K-TIG* arc, a device with magnetic field tips and water-cooled permanent magnetic poles was developed [20]. The threshold current for full penetration in the system has been reduced by 30 A, but the magnetic pole is easily damaged at high temperatures. This process can increase the penetration depth by 2–3 times when welding 304 stainless steel, but the weld metal has a higher oxygen content.

The authors applied double-shielding *TIG* welding to weld ultrathin metal plates [21]. Thus, summarizing the optimization described above, constricting the gas flow can increase the energy density of the arc and ensure welding process stability. In double-shielding *TIG* welding, the internal gas flow must be high enough to enhance arc melting capability; otherwise, the external active gas will increase the oxygen content in the weld metal. Further improvements are needed to make more efficient use of the internal gas flow.

Currently, many technical solutions have been proposed to increase the energy efficiency of TIG welding. Based on the available literature [6–35], two directions for increasing arc energy density were identified. The first is control and reduction of the arc space, i.e., compression and constriction of the arc. The second is an increase in the number and energy of particles in the arc. The main methods for achieving the above-mentioned goals include: adding energy to the arc, changing the ionization of the arc, and increasing the heat transfer of the arc.

For example, multi-electrode *TIG* welding (*MT-TIG*) includes two-electrode *TIG* welding (*T-TIG*), condensation *TIG* welding (*C-TIG*), and *MT-TIG* [34, 35]. Typical characteristics of these methods are the use of two, three, or more tungsten electrodes isolated from each other in an aligned array, instead of a single traditional tungsten electrode. Several power sources are connected to the groups of tungsten electrodes, and a connecting arc is formed between the electrodes. The required arc characteristics are achieved through logical control between multiple power sources to meet the requirements of high-efficiency surfacing and high-speed welding.

The keyhole *TIG* welding method (*K-TIG*) [35] was proposed by the *Commonwealth Scientific and Industrial Research Organisation* (*CSIRO*) in 1997. The principle of *K-TIG* is to use a special energy source for arc welding with a unique welding torch design, namely, a large-diameter tungsten electrode (usually more than 6 mm), high current (> 600–650 A), and high voltage (16–20 V). As a result, the arc is constricted, the energy density increases significantly, and the penetration depth increases [35].

C-TIG is a new arc welding method [35] in which the arc is protected by two layers of shielding gas: inner and outer. Three parallel tungsten electrodes are powered by three independent power sources. Properly designed deflecting tungsten electrodes are used to guide the arc so that three parallel arcs converge into one. The current of the coupled arc formed by three parallel arcs is equivalent to the sum of the currents of the three tungsten electrodes; therefore, the total welding current can be extremely large.

At the same time, the high temperature generated by a strong current increases thermal ionization of the gas in the arc center and thermionic emission at the electrode; in addition, the arc energy increases significantly. In combination with thermal compression and the constraining effect of the outer shielding gas, the energy density of the arc is further increased.

Another way to increase TIG welding efficiency is to use additional physicochemical effects on the weld pool via activating fluxes [6–15]. The first work in this direction was carried out in the *USSR* [6–15]. Titanium was used as the material to be welded, and the penetration depth was significantly increased. The disadvantage is that TIG welding only allows joining of thin titanium sheets in a single pass. Joining thick plates requires machining grooves and feeding filler material. The deposition rate is low, and the grains in the melting zone tend to coarsen, which leads to deterioration of the joint properties. Subsequently, this positive experience was extended to structural and stainless steels. In this process, a thin layer of flux is applied to the surface to be welded, after which TIG welding is performed. Oxides, chlorides, and fluorides are commonly used as fluxes in this process. Fluxes are applied to the surface after mixing with a suitable solvent such as acetone or ethanol, in an appropriate proportion using a brush or spray.

The primary effect of using flux during *TIG* welding is a noticeable increase in arc voltage [6, 7]. Traditionally, during *TIG* welding, the arc voltage increases with arc length. For example, at an arc length of 2.5 mm, the voltage is 9.8–10 V, while at an arc length of 10 mm, it reaches 14.5–14.8 V. However, increasing the arc length during *TIG* welding degrades weld pool shielding and increases shielding gas consumption.

According to the results of a large number of published works [6–25], *A-TIG* welding successfully provides a large depth of penetration (*DOP*) for various materials, including carbon steel [6–8], titanium alloys [6–10], and stainless steels [5–15], etc. In addition, new variants of *FB-TIG* and *FZ-TIG* have recently been developed and experimentally investigated [22–24] by changing the geometric arrangement of fluxes on the surface of the metal being welded.

In *FB-TIG* welding, two flux strips are applied on both sides of the weld centerline, leaving a small gap in the center of the plate. In *FZ-TIG* welding, a flux layer with a high melting point, high boiling point, and low electrical conductivity is applied to the side surfaces of the weld, while the central areas are coated with a flux layer having a low melting point, low boiling point, and high electrical conductivity [22–28].

In [25], a comparative study of the effect of single-component fluxes (MoO_3 and *MgO*) on the depth-to-width ratio (*DWR*) of oxygen-free copper was conducted using new *A-TIG* welding options. An increase in penetration depth was observed.

Recently, new methods, *FB-TIG* and *FZ-TIG* (*A-TIG* welding variants), have also been studied in the context of improving *DWR* and overall weld properties. The authors of [25] showed that *FB-TIG* welding of *AA 2219-T87* aluminum alloy using SiO_2 flux produces aesthetically better welds without cracks and with the formation of liquid slag compared to traditional TIG methods. In addition, the tensile strength and yield strength of the weld improved significantly, by 50–54%.

A study of *FB*-T*I*G [26] on commercially pure aluminum using fluxes with different particle sizes (SiO_2, TiO_2, Al_2O_3, Fe_2O_3, and Cr_2O_3) showed that a flux with a small particle size increases penetration by 30%

compared to a flux with large particles. In addition, the gap between the flux strips plays a crucial role in achieving high weld quality. When the gap between the flux strips was maintained in the range of 4–5 mm, the depth-to-width ratio (*DWR*) of the weld increased at least 5-fold compared to conventional *TIG* welding [6–15].

The authors of [28] consider *FZ-TIG* to be the most advanced technology, as it reportedly combines the advantages of both *A-TIG* and *FB-TIG*. They applied this new technology to aluminum alloy *A3003* using a specially made flux, *FZ108*, which contained a mixture of several halides and elements as the central flux, with SiO_2 selected as the side flux. The results unexpectedly showed that the weld penetration achieved with *FZ-TIG* was more than three times higher than that of conventional TIG welding and almost twice as high as that of *A-TIG*. Other authors [29] also reported a threefold increase in penetration depth compared to conventional *TIG* welding, with a noticeable improvement in the mechanical properties of the aluminum alloy.

A large number of authors have noted that oxide-based fluxes such as SiO_2, MoO_3, MoS_2, CrO_3, and TiO_2 significantly increase the depth of penetration (*DOP*) for various materials and, in many cases, provide full penetration (i.e., penetration through the entire plate thickness) in conventional *TIG* welding. A noticeable increase in penetration is observed when H_2 is added to the shielding gas. The addition of helium also contributes to an increase in *DOP*. The arc column narrows during activated *TIG* welding, and an inward flow caused by surface tension is observed.

Various types of welding operations and their measurement technologies have been proposed in the analyzed literature [6–49]. Some studies have described aspects of *A-TIG* weld quality measurement methods and recommendations. However, from our brief analysis of the results reported by various authors [6–49] and other scientific papers in this area, we have found no studies on new methods for welding low-carbon steel. In our previous work [50], we presented the test results of oxide fluxes during *A-TIG* welding. With this in mind, it is of scientific interest to consider the effect of activating flux placement using *FB-TIG* and *FZ-TIG* methods on the surface of the workpieces being welded.

The purpose of this work is to evaluate the penetration capability during FB-*TIG* and *FZ-TIG* welding (using *FeO*, TiO_2, and SiO_2 oxide fluxes) on carbon and low-alloy steels. To achieve this goal, ***the following tasks*** were addressed in the research process:

– to determine the technological parameters (current, flux coating thickness, welding speed) affecting penetration capability during *FB-TIG* and *FZ-TIG* welding using *FeO*, TiO_2, and SiO_2 oxide fluxes;

– to conduct a metallographic study of the structure formed in welds during *FB-TIG* and *FZ-TIG* welding using *FeO*, TiO_2, and SiO_2 oxide fluxes;

– to perform visual studies of the process using photographic recording of individual stages to establish the features of welding arc interaction with activating fluxes in *FB-TIG* and *FZ-TIG*.

Research methods and materials

In our previous work [50], we described the research methodology in detail.

Materials for the experiments

Rectangular plates with dimensions of 20 × 50 mm were cut from sheets with thicknesses of 3, 5, and 10 mm. Sixty samples were prepared for each thickness. Additional studies were carried out when weld surface formation was unsatisfactory (due to lack of fusion or poor bead formation).

The following steels were used:

– commercial quality *Steel 3* (*GOST 380-2005*) – see Table 1.

– *0.09 C-2 Mn-Si* steel (*GOST 19281-2014*) – see Table 2.

– *0.1 C-Cr-Ni-Cu* steel (*GOST 19281-2014*) – see Table3.

As in our previous work [50], single-component fluxes in the form of oxide powders (TiO_2, SiO_2, *FeO*) with a particle size of 40–80 μm, manufactured by *Real-Dzerzhinsk LLC* (Russia), were used. Additionally, silicon and ferrosilicon production waste – namely, *FeSi* gas purification dust – was used. The gas purifica-

Table 1

Chemical composition (wt.%) of *Steel 3* according to *GOST 380-2005*

C	*Si*	*Mn*	*Ni*	*S*	*P*	*Cr*	*As*	*Cu*
0.14–0.22	0.5–1.5	0.4–0.65	≤ 0.3	≤ 0.04	≤ 0.04	≤ 0.3	≤ 0.08	≤ 0.3

Table 2

Chemical composition (wt.%) of *0.09 C-2 Mn-Si* steel according to *GOST 19281-2014*

C	*Si*	*Mn*	*Ni*	*S*	*P*	*Cr*	*V*	*Cu*
≤ 0.12	0.5–0.8	1.3–1.7	≤ 0.3	≤ 0.035	≤ 0.03	≤ 0.3	≤ 0.12	≤ 0.3

Table 3

Chemical composition (wt.%) of *0.1 C-Cr-Ni-Cu* steel according to *GOST 19281-2014*

C	*Si*	*Mn*	*Ni*	*S*	*P*	*Cr*	*V*	*Cu*
≤ 0.12	0.8–1.1	0.5–0.8	0.5–0.8	≤ 0.035	≤ 0.03	0.6–0.9	≤ 0.12	0.4–0.6

tion dust from silicon and ferrosilicon production consists of the following oxides: SiO_2 – 85.4%, Al_2O_3 – 10.46%, Fe_2O_3 – 0.30%, *CaO* – 1.50%, *MgO* – 1.24% [14]. Before welding, the samples were cleaned with a belt grinder and then wiped with acetone to prevent surface contamination.

Welding procedure

The welding experiments were conducted as follows: the welding current was varied in the range of 80–250 A, while the welding speed was kept constant at 100 mm/min. The welding voltage was set at 15 V. A *MasterTig 300 AC/DC* welding power source (Finland) was used. Thermal energy was calculated using a standard formula, assuming a heat transfer efficiency of 0.8 [6–8]. High-purity argon was used as a shielding gas in accordance with *GOST 10157-2016*. The gas flow rate was set at 20 L/min. The flux components were optimized in an earlier study [50].

The finely dispersed flux powders were dispersed in acetone; the resulting solution, which resembled paint in consistency, was subsequently applied to the sample surfaces using a stencil template. The coating thickness varied from 0.5 to 2 mm.

Metallographic examination

After welding, the samples were sectioned along the entire length of each weld using a *STRUERS SECOTOM-15* cutting machine (Denmark) for metallographic examination. Hot pressing was carried out using *FlexPRESS-600* equipment. The samples were carefully polished using a semi-automatic machine (*Struers Labopol*, Denmark). Fine polishing was carried out sequentially using a suspension of aluminum oxide and diamond to obtain a mirror surface. The surface was etched with a 4 vol.% nitric acid solution.

Micrographs of the weld zone were obtained using an optical microscope (*Micromed MET 2*, China). A general macroscopic view of the weld zone and the heat-affected zone (*HAZ*) was obtained using a stereo microscope (*Olympus SZX16*). All measurements concerning weld geometry were carried out using *ImageJ* software.

The methodology adopted for the experimental work is shown in Fig. 1.

To obtain information about microstructural characteristics during the welding process, various additional measurement methods were used, such as high-speed photography using a *Nikon Z30* camera (capable of shooting 4K video at up to 30 fps) and recording of current and voltage parameters using a welding parameter recorder (*RSP-102D*).

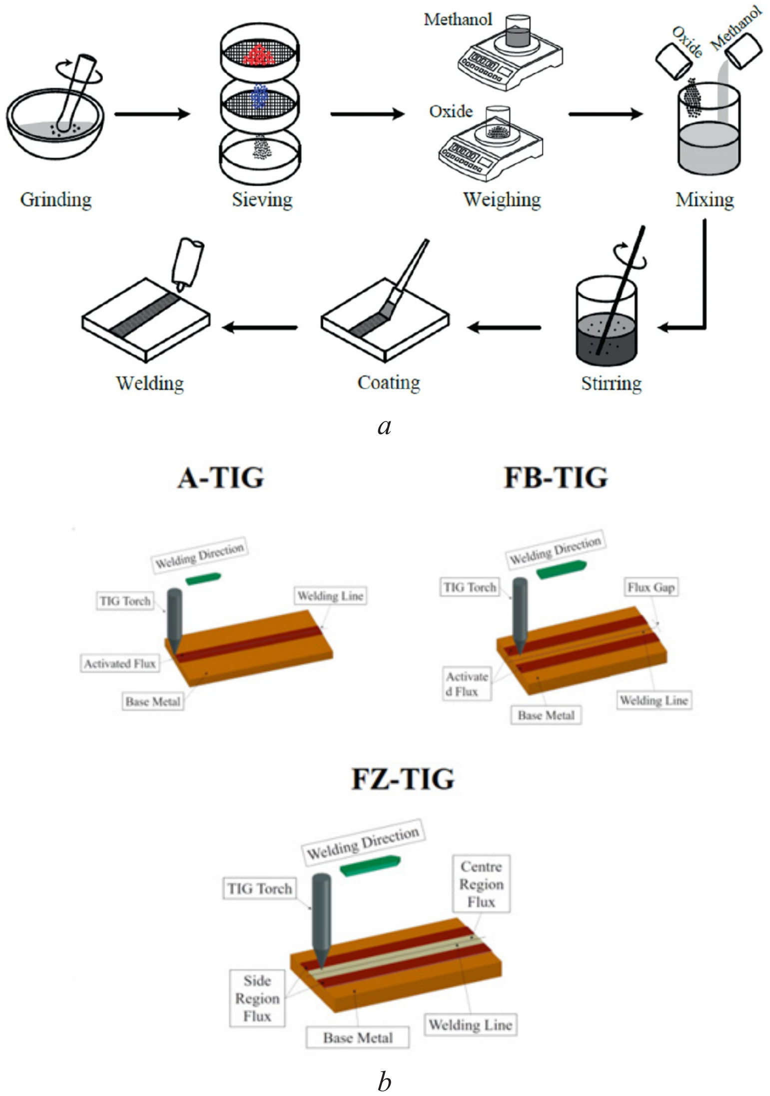

Fig. 1. (*a*) Procedure for preparing activated flux [50] and (*b*) schematic representation of variants of new *A-TIG* welding methods with activated flux

The variants of *FB-TIG* and *FZ-TIG* welding were experimentally investigated by changing the geometric arrangement of the fluxes. In *FB-TIG* welding, two flux strips were applied on both sides of the weld centerline, leaving a small gap in the center of the plate (Fig. 1, *a*). In *FZ-TIG* welding, a flux layer with a high melting point, high boiling point, and low electrical conductivity (e.g., SiO_2) was applied to the lateral and central sections of the weld surface, while a flux layer with a low melting point, low boiling point, and high electrical conductivity (e.g., CaO, Al_2O_3) was applied to other areas (Fig. 1, *b*).

For each current value and welding method, at least three samples were tested. Next, the average value of the geometric parameters was determined.

Research results

A macrographic view of the melting zone with and without activating flux is shown in Figs. 2–5. The boundary of the melting zone is clearly visible in all images. The etched surface on some samples was so bright that it reflected light from a portable lamp used with a stereo microscope. Therefore, it was difficult to create sufficient contrast between the various microscopic areas in the macro images. The macro images confirm the absence of common welding defects such as porosity, undercuts, or cracks on the welds.

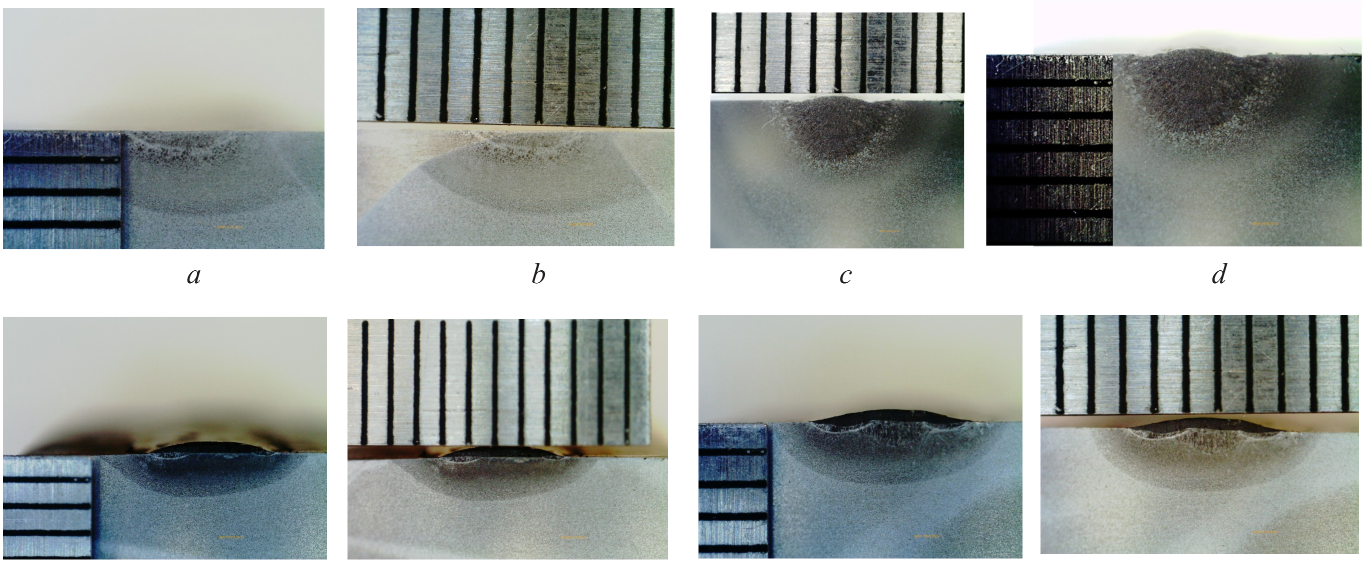

a *b* *c* *d*

e *f* *g* *h*

Fig. 2. Cross-sections of the weld zone after *FB-TIG* processing:

a – width parameter (without flux, with surface melting, penetration depth at 100 A); *b* – penetration depth parameter (without flux, with surface melting, width at 100 A); *c* – silicon oxide – weld width at 100 A; *d* – silicon oxide – penetration depth at 100 A; *e* – ron oxide – penetration depth at 120 A; *f* – iron oxide – weld width at 120 A; *g* – iron oxide – penetration depth at 150 A; *h* – iron oxide – weld width at 150 A

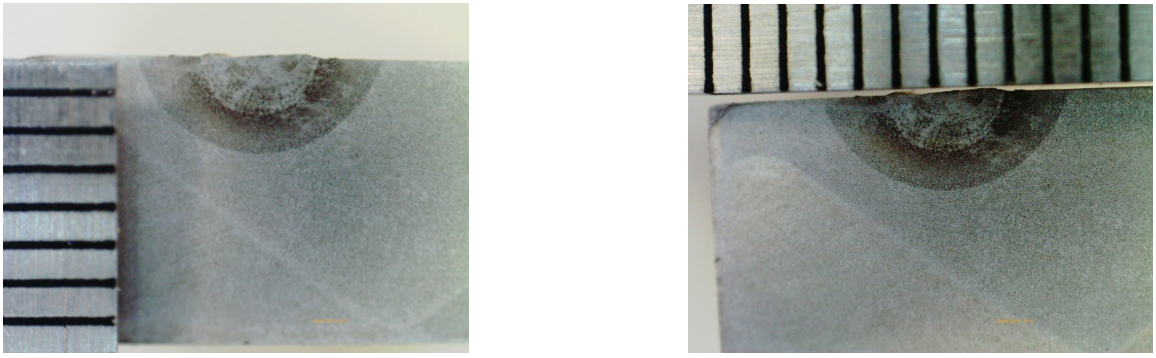

a *b*

Fig. 3. Cross-section of samples after *FB-TIG* treatment (current 100 A):

a – *FeSi* gas cleaning dust – penetration depth; *b* – *FeSi* gas cleaning dust – width

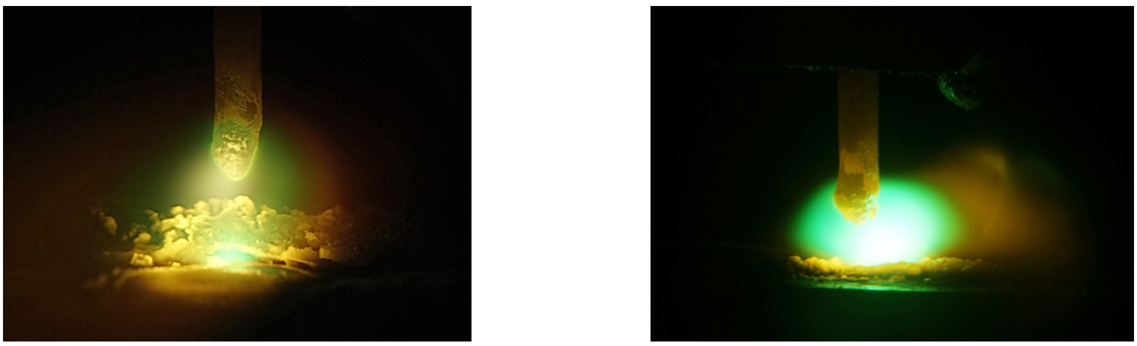

a *b*

Fig. 4. Photographs of the interaction process between the welding arc column and flux particles during welding with activated SiO_2 flux:

a – *A-TIG*; *b* – *FB-TIG* (current 100 A)

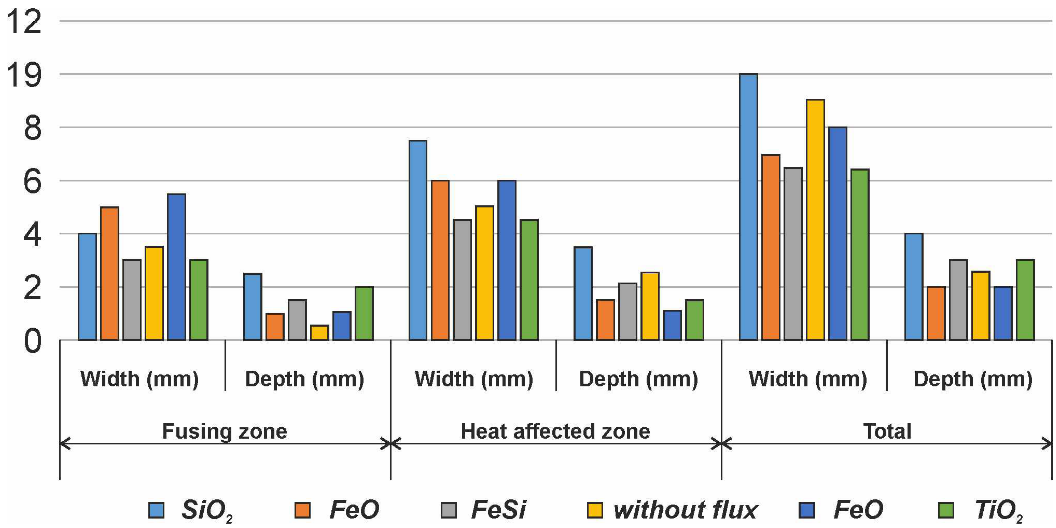

Fig. 5. Variation of width and depth in *FB-TIG* welding in the fusion zone (*FZ*), heat-affected zone (*HAZ*), and total depth

The results of penetration depth and weld width measurements during *FB-TIG* and *FZ-TIG* welding are shown in Tables 4 and 5. It can be seen that the activating flux application method significantly affects weld geometry. Typical macrostructures and micrographs of *TIG*, *A-TIG*, *FB-TIG*, and *FZ-TIG* samples include various zones – namely, the melting zone, the base metal, and the heat-affected zone (*HAZ*) – with different grain morphologies (Figs. 6, 7 and 8).

Table 4

Variation of width and depth during *FB-TIG* welding

Current, A	Flux applied to *Steel 3* (center gap of 2 mm)	Penetration depth (mm)	Penetration width (mm)
100	Without flux	1.15	5.31
100	SiO_2	2.64	5.37
100	*FeO*	0.32	4.98
120	*FeO*	0.90	5.31
100	TiO_2	1.96	4.96
Current, A	Flux applied to *Steel 3* (center gap)	Penetration depth (mm)	Penetration width (mm)
100	SiO_2, gap 4 (mm)	2.84	5.27
100	SiO_2, gap 6 (mm)	2.44	5.67
100	SiO_2, gap 8 (mm)	1.96.	6.17

Table 5

Variation of width and depth during *FZ-TIG* welding

Current, A	Flux applied to *Steel 3* (center gap of 2 mm)	Penetration depth (mm)	Penetration width (mm)
100	Without flux	1.15	5.31
100	SiO_2	2.94	5.31
100	*FeO*	0.82	4.53
120	*FeO*	1.40	5.11
100	TiO_2	2.76	5.00

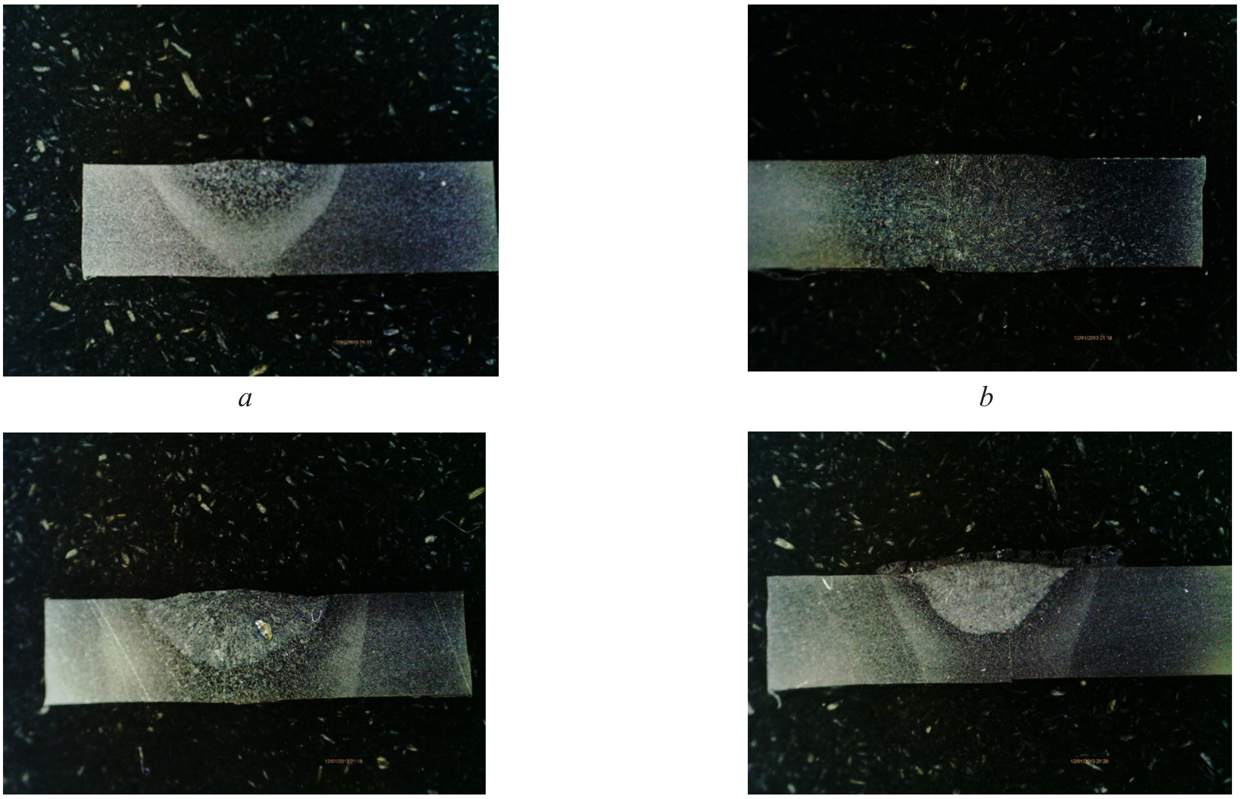

a *b* *c* *d*

Fig. 6. Transverse sections of a weld seam of a 5 mm plate without edge preparation after *FB-TIG* welding at 100 A:

a – welding without flux; *b* – welding with SiO_2; *c* – iron oxide; *d* – *FSi* gas cleaning dust

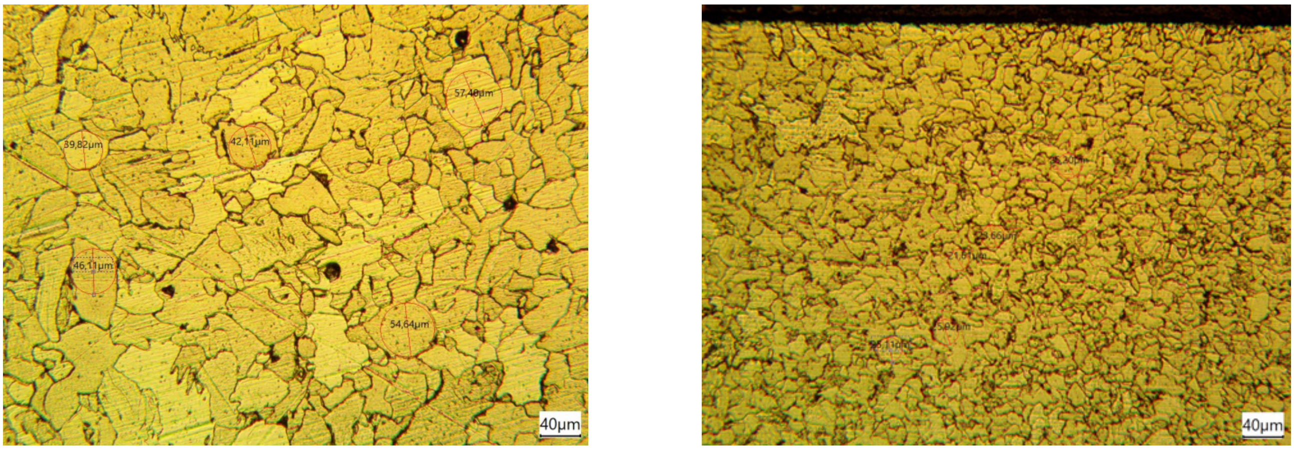

a *b*

Fig. 7. Microstructure in the coarse grain zone. Transverse sections of a weld seam of a 5 mm plate without edge preparation after welding with SiO_2 flux:

a – *A-TIG* method; *b* – *FB-TIG* method (current 100 A)

Table 6 shows the results of *FB-TIG* welding with flux coating thicknesses varying from 0.5 to 3 mm. It can be seen that the largest coating thickness (3 mm) does not allow high-quality penetration at a current of 100 A. With a coating thickness of 1 mm, the weld width is larger than with other options. With a coating thickness of 1 mm, the largest weld depth is 2.64 mm. The next largest weld depth values were obtained with an active flux coating thickness of 3 mm at a current of 140 A.

The optimal thickness of the active SiO_2 flux coating for 3–5 mm thick metal is in the range of 0.5–1 mm. Therefore, an increase or decrease in the specified thickness of the active flux coating has a

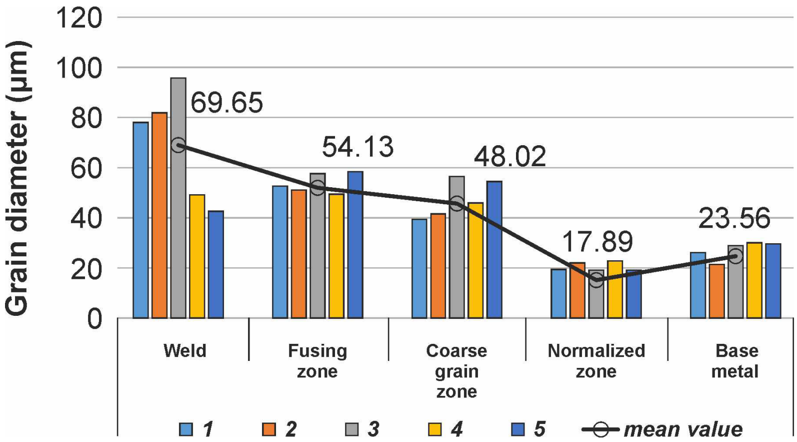

a

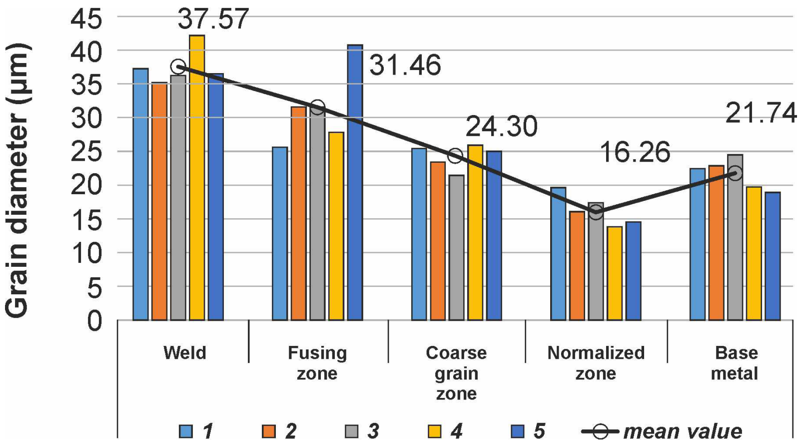

b

Fig. 8. Grain sizes of transverse sections of a weld seam of a 5 mm plate without edge preparation after welding with SiO_2 flux:
a – *A-TIG* method; *b* – *FB-TIG* method (current 100 A)

Table 6

Changing the width and depth during *FB-TIG* welding

Current, A	Flux applied to Steel 3 (center gap of 2 mm)	Coating thickness (mm)	Penetration depth (mm)	Penetration width (mm)
100	SiO_2	0.5	1.75	5.31
100	SiO_2	1.0	2.64	5.47
100	SiO_2	2.0	2.32	4.98
100	SiO_2	3.0	–	–
120	SiO_2	3.0	2.58	5.40
140	SiO_2	3.0	2.70	6.12

significant effect on the depth and width of the weld. When the active flux coating thickness exceeds the optimal value (> 1 mm), arc ignition becomes difficult, leading to shallower penetration and deterioration of surface quality. If the active flux coating thickness is less than the optimal value, no significant improvement in weld depth is observed.

Fig. 9. Shows the results of samples processed using the *FZ-TIG* method (current 100 A).

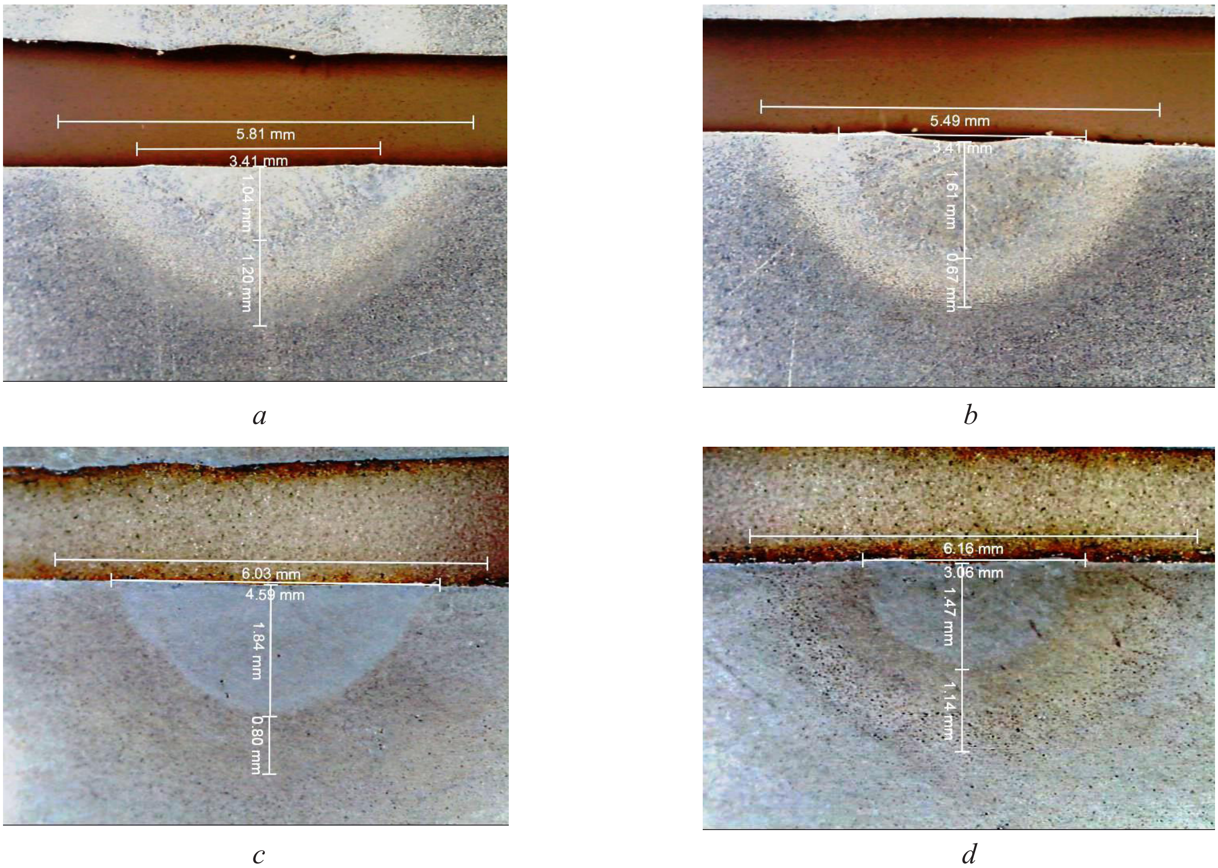

Fig. 9. Cross-sections of samples processed by the *FZ-TIG* method (current 100 A):
a – silicon oxide; *b* – titanium oxide; *c* – gas cleaning dust; *d* – iron oxide

Due to the varying physical properties of the fluxes, different voltage values were recorded during *A-TIG* and *FB-TIG* welding. *FB-TIG* and *FZ-TIG* welding produce the highest arc voltage**.** The heating intensity at the arc center increases with voltage and decreases exponentially with radial distance from the center. This leads to constriction of the arc column and an increase in heat flux density, which significantly affects penetration (Fig. 9).

A comparative assessment of the different methods is given in Fig. 10.

Discussion of the results

Our research has allowed us to identify some new features of activating fluxes. For example, a large penetration depth was observed when using silicon oxide (Fig. 2). SiO_2 flux has the highest electronegativity among all oxide fluxes. As a result, the dissociation of oxide fluxes attracts more electrons to the outer region of the arc column than to the center. The electrons gather on the outer periphery of the arc, leading to increased arc constriction. In addition, metal oxides are more basic and strongly bound to oxygen, making the decomposition of basic oxides difficult. In contrast, acidic compounds decompose easily, releasing more free energy and achieving greater penetration depth.

The greater penetration depth achieved using oxide fluxes can be explained by two possible mechanisms: arc column constriction and the *Marangoni* effect. In general, as our previous studies [50] have shown, penetration depth in traditional *TIG* welding depends on the fluid flow mode in the weld pool. This, in turn, strongly depends on factors such as electromagnetic forces and the surface tension gradient. Fig. 4 shows the change in arc column shape during *A-TIG* and *FB-TIG* welding. The *A-TIG* and *FB-TIG* visualizations are shown in the photograph. It can be seen that when the arc burns through the flux layer, it is in continuous contact with the flux particles. In the *FB-TIG* method, the arc is constricted by the side walls of the flux, which are not electrically conductive.

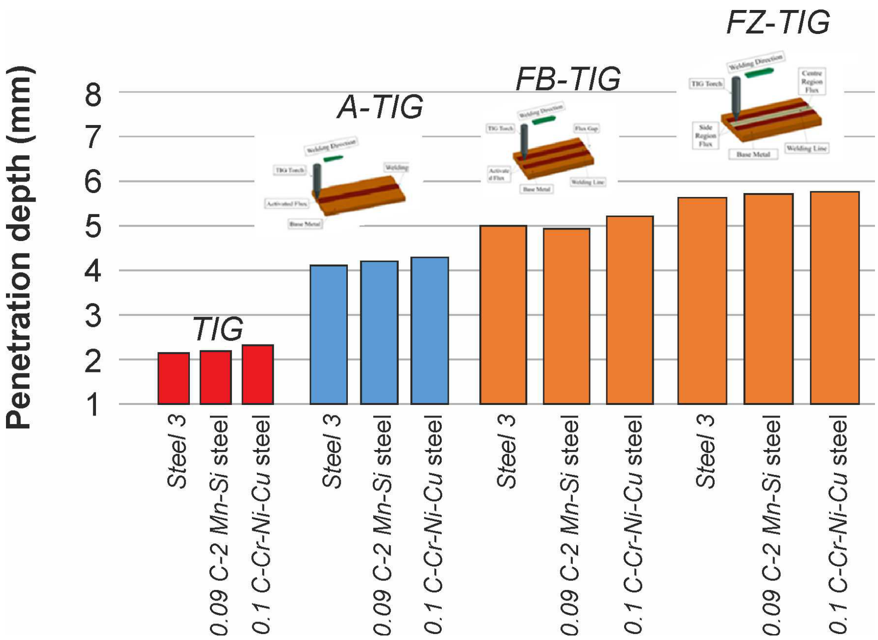

Fig. 10. Penetration depth as a function of steel chemical composition (plate thickness 10 mm, current 200 A) for various activated flux *TIG* welding methods

Fig. 5 shows the variation in weld width and penetration depth for different fluxes. SiO_2 and TiO_2 fluxes have a stronger effect on these weld parameters than others. The authors [6–8, 12–19] reported that activated flux ionizes during welding and constricts the arc, trapping electrons in the outer and central regions of the arc. Subsequently, the anode current density increases, which leads to an increase in the heat flow in the spot and to a narrower and deeper weld.

However, many researchers believe that the main reason for the increase in weld depth is reverse (centripetal) *Marangoni* convection. The addition of activating flux increases the surface tension gradient in the central part compared to the outer edges, causing the molten metal to flow toward the center and increasing penetration depth.

The *TIG* welding sample without flux showed a columnar grain structure in the weld area (Fig. 7,*a*). It is worth noting that the samples treated with *A-TIG* and *FZ-TIG* showed long needle-like grains, while the samples treated with *FB-TIG* showed cellular grains in the weld area. This is important because the weld area undergoes cyclic rapid heating during *A-TIG* and *FZ-TIG*, as the weld is covered with flux, which leads to a high current density and strong Marangoni convection. However, the presence of a constricted arc created by lateral flow, but with a current density limited to almost that of *TIG* welding, leads to moderate heating of the melting zone followed by slow cooling, which allows the grains to grow into a cellular structure.

In TIG welding, in the absence of such mechanisms, the melting zone undergoes slow heating and cooling cycles, leading to the formation of a columnar structure (Fig. 7,*a*). In addition to the melting zone, the heat-affected zone (*HAZ*) mainly consists of a very fine-grained morphology due to faster cooling caused by heat flow to the cold base metal. Microstructural analysis of the samples revealed defects such as porosity in varying degrees of severity in the weld area.

Reference [15] suggests that during *A-TIG* welding, oxygen released during the decomposition of the oxide flux dissolves in the molten metal and can escape into the environment after solidification. It can be argued that the amount of porosity depends on the oxide present in the flux. In many cases during *FB-TIG* welding, the arc is not confined solely by its natural radius, especially when the lateral flux layer has limited electrical resistance. This increases the flow of liquid into the weld pool, transferring activating flux particles to the central area. This influx of particles helps to increase penetration depth but simultaneously leaves behind voids formed by oxygen released from the flux, as described earlier. The samples welded without flux also showed porosity and larger voids in the weld area. Therefore, it can be assumed that there are several reasons for the formation of porosity during *TIG* welding. It is known [6–8] that the absorption of nitrogen and oxygen in the weld pool is usually caused by poor gas shielding.

From the works of various authors [6–49], it is evident that the phenomenon of increased penetration depth using activating fluxes is complex. No complete analysis has yet been presented; only individual studies have investigated specific cases, offering various explanatory mechanisms. These mechanisms include arc constriction, the reverse *Marangoni* effect [15], electromagnetic forces [6–9], and buoyancy and aerodynamic forces [6, 12, 21–22].

From the experimental results of this study, it is clear that each flux has unique chemical, thermal, and electrical properties, leading to different weld geometries due to one or more of these mechanisms. Fig. 10 shows a comparative assessment of various methods. It can be seen that, compared to conventional *TIG* welding, the use of activating fluxes increases penetration depth regardless of the application method. The geometric dimensions of the bead-on-plate samples made of carbon and low-alloy steel confirmed a significant increase in penetration depth, which correlates with the work of other authors [6–19].

Continuous linear spatter was observed on the upper surface of samples welded by the *A-TIG* method using fluxes such as SiO_2, TiO_2, and *FeO*. Such excessive spatter when using these fluxes could be caused by strong arc constriction due to a higher peak temperature during processing.

During *A-TIG* welding, electron movement is hindered by the flux deposited on the weld centerline [6–8], since most fluxes are good electrical insulators. Since electrons take the path of least resistance (i.e., along the sides), this leads to arc wandering and consequent spatter. Consequently, *A-TIG* welding creates more surface inhomogeneities compared to *TIG* welding, which is explained by the inevitable formation of residual slag spatter [6–8]. Fewer spattering was observed when using fluxes, which is explained by the formation of a slag layer from the flux applied before welding.

In *FB-TIG* welding, the opposite situation occurs: the central area remains uncoated, while the lateral areas are covered. This leads to better arc control and its constriction in the center. Therefore, comparatively less spatter was observed in the *FB-TIG* welding samples.

During *FZ-TIG* welding, a significant amount of spatter was observed on the weld surface, which is explained by strong arc constriction and high arc energy density. During *FZ-TIG* welding, a flux with high electrical conductivity is applied in the center of the seam, which provides a path of minimal electrical resistance for the arc column. The side parts, in contrast, contain flux particles with low electrical conductivity and are exposed to the convective thermal action of the arc column.

It was reported in [6–8] that the electronegativity of flux components plays a key role in arc characteristics and heat generation. During *A-TIG* and *FZ-TIG* welding, decomposition of the oxide flux leads to the release of the metallic element and oxygen. The properties of the oxide can be described by the electronegativity of a given element in combination with oxygen. Negative ions formed by electron aggregation at the arc periphery can lead to arc constriction. The addition of activating fluxes with a high melting point to the weld center causes higher surface tension there [15]. A higher surface tension in the center and a lower one at the edges directs molten metal flow toward the center rather than outward, as in conventional *TIG* welding. This mechanism – the reverse surface tension gradient leading to narrow and deep penetration – is called the reverse *Marangoni* convection effect and is well explained in [15]. Therefore, more than one mechanism likely contributes to increased weld penetration.

It should be noted that the mechanism described above is slightly different for *FB-TIG* welding, as the flux application location changes. When the arc is ignited, in addition to the central region, it also interacts with flux particles in the lateral regions. Intense heating dissociates the flux particles, leading to evaporation and the formation of a vapor cloud outside the arc column. The interaction between the vapor cloud particles and adjacent electrons – which have lower energy than those in the central region – prevents further arc expansion. Thus, with such a constricted arc, higher penetration depth is observed in our experiments.

The samples obtained using the *FZ-TIG* method exhibited a combination of the mechanisms discussed earlier, since this is a combined approach incorporating characteristics of both *A-TIG* and *FB-TIG* welding.

Consequently, these samples showed a narrower weld with a higher penetration depth-to-width ratio compared to both of the above approaches.

When welding using the *FB-TIG* method, the gap between the fluxes has a significant effect on increasing penetration depth and reducing weld width, as shown in Table 4. During the experiments, it was found that as the gap between the fluxes decreases, the penetration depth increases, leading to a greater depth-to-width ratio compared to conventional *TIG* welding.

This observation can be explained by the fact that in *TIG* welding, the energy required to melt the base metal is obtained from kinetic energy transferred to charged particles (electrons or positively charged ions). The resistance of the silica flux coating is significantly higher than that of the base metal. Consequently, electron flow is confined to the flux-free area – i.e., inside the gap between the fluxes [15]. This phenomenon is known as the *isolation effect*.

The depth and shape of the weld significantly depend on the molten metal flow and liquid flow mode in the welding zone. For pure metals and alloys, surface tension ($\boldsymbol{\sigma}$) decreases with increasing temperature ($\boldsymbol{T}$). Thus, the center of the weld pool, which receives maximum heat from the welding torch, has minimal surface tension compared to the outer edges, creating a significant surface tension gradient. This causes molten metal to flow from the center (lower surface tension) to the periphery (higher surface tension) [6–14].

As the flux gap gradually decreases, the concentration of the activating element (oxygen) in the molten weld pool increases. The silicon dioxide particles adjacent to the weld pool melt due to intense heating, causing the temperature coefficient of surface tension to change from negative to positive. This leads to an increase in surface tension ($\boldsymbol{\sigma}$) with temperature at the weld pool center, where the maximum temperature occurs. As a result, the molten metal flow direction is reversed – a phenomenon known as reverse *Marangoni* flow or reverse *Marangoni* convection – leading to greater weld penetration and reduced weld width [6–8]. Thus, the weld pool becomes deep and narrow rather than wide and shallow.

In conclusion, the spatial distribution of arc current density and the interaction of thermal, electrical, and other physical parameters significantly impact the geometric dimensions and metallurgical quality of the weld. In our studies, arc heat flux density can be characterized by current density distribution. We adjusted these parameters by applying activating fluxes to the surface using various methods. Considering these features of the welding process, we have outlined further studies to evaluate the penetration capability of new methods for using activating fluxes in *TIG* welding.

Conclusions

The main results can be summarized as follows:

1. In the course of research on new *FB-TIG* and *FZ-TIG* methods, it has been shown that SiO_2 and TiO_2 fluxes not only increase weld penetration depth but also improve weld pool control. The complex flux made from gas purification dust (consisting of oxides: SiO_2 – 85.4 %, Al_2O_3 – 10.46 %, Fe_2O_3 – 0.30 %, CaO – 1.50 %, MgO – 1.24 %) increases penetration depth but is less efficient than simple fluxes such as SiO_2 and TiO_2. The penetration depth during *FB-TIG* welding increases with flux coating thickness up to 1 mm, after which it remains constant over a wide range of welding currents.

2. A difference in the heat-affected zone (*HAZ*) microstructure has been established: *A-TIG* welding produces a larger grain structure (65–76 μm), whereas *FB-TIG* welding produces a smaller one (35–45 μm). The grain size in the weld area during *FB-TIG* welding is half that observed during *A-TIG* welding.

3. For welding 10 mm thick metal, the following parameters were found to achieve maximum penetration depth: welding current – 200 A, welding speed – 100 mm/min, and shielding gas flow rate – 20 L/min.

4. Visualization of *FZ-TIG* and *FB-TIG* qualitatively showed that when the arc burns through a layer of electrically conductive flux, it remains in continuous intimate contact with the flux particles and is additionally constricted by the side walls of the flux (which are not electrically conductive). As a result, the heat flux density is higher. In *FB-TIG* welding, the arc is constricted only by the side walls of the flux (not along the weld axis), so the degree of constriction is lower.

References

1. Zhang Y.M., Jiang M., Lu W. Double electrodes improve GMAW heat input control. *Welding Journal*, 2004, vol. 83 (11), pp. 39–41.

2. Xiang R., Huang J., Yu X., Zhao H., Fan D. A review of double-electrode GMAW: Approaches, developments and variants. *Journal of Manufacturing Processes*, 2025, vol. 133, pp. 1160–1182. DOI: 10.1016/j.jmapro.2024.12.017.

3. Modenesi P.J. The chemistry of TIG weld bead formation. *Welding International*, 2015, vol. 29 (10), pp. 771–782. DOI: 10.1080/09507116.2014.932990.

4. Gurevich S.M., Zamkov V.N., Kushnirenko N.A. Improving the penetration of titanium alloys when they are welded by argon tungsten arc process. *Automatic Welding*, 1965, vol. 18 (9), pp. 1–5.

5. Liu F., Liu Z., Zhang W. Arc characteristics and welding state in gas-focusing TIG. *The International Journal of Advanced Manufacturing Technology*, 2023, vol. 129, pp. 5335–5346. DOI: 10.1007/s00170-023-12631-3.

6. Paton B.E., Zamkov V.N., Prilutsky V.P., Poritsky P.V. Kontraktsiya dugi flyusom pri svarke vol'framovym elektrodom v argone [Arc contraction by flux during tungsten electrode welding in argon]. *Avtomaticheskaya svarka = Automatic Welding*, 2000, no. 1, pp. 3–9.

7. Savitsky M.M., Kushnirepko B.N., Oleynik O.N. Osobennosti svarki stalei vol'framovym elektrodom s aktiviruyushchimi flyusami [Features of welding steels with a tungsten electrode with activating fluxes]. *Avtomaticheskaya svarka = Automatic Welding*, 1999, no. 12, pp. 18–22.

8. Jayakrishnan S., Chakravarthy P. Flux bounded tungsten inert gas welding for enhanced weld performance – A review. *Journal of Manufacturing Processes*, 2017, vol. 28, pp. 116–130. DOI: 10.1016/j.jmapro.2017.05.023.

9. Bhanu V., Gupta A., Pandey C. Role of A-TIG process in joining of martensitic and austenitic steels for ultra-supercritical power plants-a state of the art review. *Nuclear Engineering and Technology*, 2022, vol. 54 (8), pp. 2755–2770. DOI: 10.1016/j.net.2022.03.003.

10. Pandya D., Badgujar A., Ghetiya N. A novel perception toward welding of stainless steel by activated TIG welding: a review. *Materials and Manufacturing Processes*, 2021, vol. 36 (8), pp. 877–903. DOI: 10.1080/10426914.2020.1854467.

11. Fande A.W., Taiwade R.V., Raut L. Development of activated tungsten inert gas welding and its current status: A review. *Materials and Manufacturing Processes*, 2022, vol. 37 (8), pp. 841–876. DOI: 10.1080/10426914.2022.2039695.

12. Tanaka M., Shimizu T., Terasaki T., Ushio M., Koshiishi F., Yang C.-L. Effects of activating flux on arc phenomena in gas tungsten arc welding. *Science and Technology of Welding and Joining*, 2000, vol. 5 (6), pp. 397–402. DOI: 10.1179/136217100101538461.

13. Babkin A.S., Kotov N.S., Terekhov V.V. Vliyanie aktiviruyushchikh flyusov na kharakteristiki elektricheskoi dugi i kachestvo shvov pri svarke austenitnykh stalei [The influence of activating fluxes on the characteristics of the electric arc and the quality of seams in welding austenitic steels]. *Izvestiya TulGU. Tekhnicheskie nauki = Bulletin of Tula State University. Technical Sciences*, 2022, no. 10, pp. 507–514. DOI: 10.24412/2071-6168-2022-10-507-514.

14. Ivanchik N.N., Balanovsky A.E., Kondratyev V.V., Tyutrin A.A. Issledovaniya produktov pererabotki otkhodov kremniya v kachestve ul'tradispersnykh aktiviruyushchikh flyusov dlya dugovoi svarki [Research of silicon waste processing products as ultradispersed activating fluxes for arc welding]. *Zhurnal Sibirskogo federal'nogo universiteta. Tekhnika i tekhnologii = Journal of Siberian Federal University. Engineering and Technologies*, 2018, no. 11 (2), pp. 155–167. DOI: 10.17516/1999-494X-0019.

15. Parshin S.G. *Nanostrukturirovannye i aktiviruyushchie materialy dlya dugovoi svarki* [Nanostructured and activating materials for arc welding]. St. Petersburg, Polytechnic University Publ., 2020. DOI: 10.18720/SPBPU/2/si20-888.

16. Liu Z.M., Cui S., Luo Z., Zhang C., Wang Z., Zhang Y. Plasma arc welding: Process variants and its recent developments of sensing, controlling and modeling. *Journal of Manufacturing Processes*, 2016, vol. 23, pp. 315–327. DOI: 10.1016/j.jmapro.2016.04.004.

17. Teker T., Özdemir N. Weldability and joining characteristics of AISI 430/AISI 1040 steels using keyhole plasma arc welding. *The International Journal of Advanced Manufacturing Technology*, 2012, vol. 63 (1), pp. 117–128. DOI: 10.1007/s00170-011-3890-5.

18. Sahoo A., Tripathy S. Development in plasma arc welding process: a review. *Materials Today: Proceedings*, 2021, vol. 41, pp. 363–368. DOI: 10.1016/j.matpr.2020.09.562.

19. Li T., Yang X.M., Chen L., Zhang Y., Cheng Lei Y., Chun Y.J. Arc behaviour and weld formation in gas focusing plasma arc welding. *Science and Technology of Welding and Joining*, 2020, vol. 25 (4), pp. 329–335. DOI: 10.1080/13621718.2019.1702284.

20. Liu Z., Chen S., Yuan X., Zuo A., Zhang T., Luo Z. Magnetic-enhanced keyhole TIG welding process. *The International Journal of Advanced Manufacturing Technology*, 2018, vol. 99 (1), pp. 275–285. DOI: 10.1007/s00170-018-2501-0.

21. Manh N.H., Le Duy H., Akihisa M., Le V.T., Ngoc T.Q., Gandham B. Development of a novel GTAW process for joining ultra-thin metal sheets. *Journal of Manufacturing Processes*, 2022, vol. 80, pp. 683–691. DOI: 10.1016/j.jmapro.2022.06.043.

22. Sire S. New perspectives in TIG welding of aluminium through flux application. *Proceedings of the 7th International Symposium*, Kobe, Japan, 2001, pp. 113–118.

23. Huang Y., Fan D., Shao F. Alternative current flux zoned tungsten inert gas welding process for aluminium alloys. *Science and Technology of Welding and Joining*, 2012, vol. 17 (2), pp. 122–127. DOI: 10.1179/1362171811 Y.0000000087.

24. Konstantinova M.V., Balanovskiy A.E., Gozbenko V.E., Kargapoltsev S.K., Karlina A.I., Shtayger M.G., Guseva E.A., Kuznetsov B.O. Application of plasma surface quenching to reduce rail side wear. *IOP Conference Series: Materials Science and Engineering*, 2019, vol. 560 (1), p. 012146. DOI: 10.1088/1757-899X/560/1/012146.

25. Rana H., Badheka V., Patel P., Patel V., Li W., Andersson J. Augmentation of weld penetration by flux assisted TIG welding and its distinct variants for oxygen free copper. *Journal of Materials Research and Technology*, 2021, vol. 10, pp. 138–151. DOI: 10.1016/j.jmrt.2020.12.009.

26. Babu A.S., Giridharan P.K., Narayanan P.R., Narayana Murty S.V.S., Sharma V.M.J. Experimental investigations on tensile strength of flux bounded TIG welds of AA2219-T87 aluminum alloy. *Journal of Advanced Manufacturing Systems*, 2014, vol. 13 (2), pp. 103–112. DOI: 10.1142/S0219686714500073.

27. Jayakrishnan S., Chakravarthy P., Muhammed Rijas A. Effect of flux gap and particle size on the depth of penetration in FBTIG welding of aluminium. *Transactions of the Indian Institute of Metals,* 2017, vol. 70 (5), pp. 1329–1335. DOI: 10.1007/s12666-016-0929-1.

28. Kondratiev V.V., Karlina A.I., Guseva E.A., Konstantinova M.V., Kleshnin A.A. Processing and application of ultra disperse wastes of silicon production in construction. *IOP Conference Series: Materials Science and Engineering*, 2018, vol. 463 (3), p. 032068. DOI: 10.1088/1757-899X/463/3/032068.

29. Yong H., Feng S., Ding F., Tao L. Flux zoned activating TIG welding of aluminum alloys. *Welding and Joining-Harbin*, 2007, vol. 5, pp. 47–49. (In Chinese).

30. Martyushev N.V., Skeeba V.Yu. The method of quantitative automatic metallographic analysis. *Journal of Physics: Conference Series*, 2017, vol. 803 (1), p. 012094. DOI: 10.1088/1742-6596/803/1/012094.

31. Voropai N.M., Lebedeva O.V., Boyko V.P. Fizicheskie svoistva svarochnykh shlakov na osnove TiO2, obrazuyushchikhsya pri plavlenii aktivirovannykh provolok [Physical properties of welding slags based on TiO_2, formed during melting of activated wires]. *Avtomaticheskaya svarka = Automatic Welding*, 1989, no. 3, pp. 19–23.

32. Zhang R.H., Pan J.L., Katayama S. The mechanism of penetration increase in A-TIG welding. *Frontiers of Materials Science*, 2011, vol. 5, pp. 109–118. DOI: 10.1007/s11706-011-0125-5.

33. Singh S.R., Khanna P. A-TIG (activated flux tungsten inert gas) welding: – A review. *Materials Today: Proceedings*, 2021, vol. 44, pp. 808–820. DOI: 10.1016/j.matpr.2020.10.712.

34 Wu H., Chang Y., Mei Q., Liu D. Research advances in high-energy TIG arc welding. *The International Journal of Advanced Manufacturing Technology*, 2019, vol. 104, pp. 391–410. DOI: 10.1007/s00170-019-03918-5.

35. Balanovskiy A.E. Digital visualisation of the process of heating and melting of metal in arc discharge with a non-consumable electrode. *Welding International*, 2017, vol. 31 (6), pp. 467–476. DOI: 10.1080/09507116.2016.1268765.

36. Narayanan R., Rameshkumar K., Sumesh A., Shankar B., Thekkuden D.T. Effect of Nano TiO_2 flux on depth of penetration and mechanical properties of TIG-welded SA516 Grade 70 steel joints – An experimental investigation. *Metals*, 2025, vol. 15 (4), p. 399. DOI: 10.3390/met15040399.

37. Tseng K.H., Lin P.Y. UNS S31603 stainless steel tungsten inert gas welds made with microparticle and nanoparticle oxides. *Materials*, 2014, vol. 7 (6), pp. 4755–4772. DOI: 10.3390/ma7064755.

38. Mamadaliev R.A., Bakhmatov P.V., Martyushev N.V., Skeeba V.Y., Karlina A.I. Influence of welding regimes on structure and properties of steel 12KH18N10T weld metal in different spatial positions. *Metallurgist*, 2022, vol. 65 (11–12), pp. 1255–1264. DOI: 10.1007/s11015-022-01271-9.

39. Balanovskiy A.E., Astafyeva N.A., Kondratyev V.V., Karlina A.I. Study of mechanical properties of C-Mn-Si composition metal after wire-arc additive manufacturing (WAAM). *CIS Iron and Steel Review*, 2021, vol. 22, pp. 66–71. DOI: 10.17580/cisisr.2021.02.12.

40. Karlina A.I., Karlina Y.I., Kondratiev V.V., Kononenko R.V., Breki A.D. Study of wear of an alloyed layer with chromium carbide particles after plasma melting. *Crystals*, 2023, vol. 13 (12), p. 1696. DOI: 10.3390/cryst13121696.

41. Kolosov A.D., Gozbenko V.E., Shtayger M.G., Kargapoltsev S.K., Balanovskiy A.E., Karlina A.I., Sivtsov A.V., Nebogin S.A. Comparative evaluation of austenite grain in high-strength rail steel during welding, thermal processing and plasma surface hardening. *IOP Conference Series: Materials Science and Engineering*, 2019, vol. 560, p. 012185. DOI: 10.1088/1757-899X/560/1/012185.

42. Malushin N.N., Gizatulin R.A., Martyushev N.V., Valuev D.V., Karlina A.I., Kovalev A.P. Strengthening of metallurgical equipment parts by plasma surfacing in nitrogen atmosphere. *Metallurgist*, 2022, vol. 65 (11–12), pp. 1468–1475. DOI: 10.1007/s11015-022-01292-4.

43. Nokhrina O.I., Gizatulin R.A., Golodova M.A., Proshunin I.E., Valuev D.V., Martyushev N.V., Karlina A.I. Alloying and modification of iron-carbon melts with natural and man-made materials. *Metallurgist*, 2022, vol. 65 (11–12), pp. 1429–1448. DOI: 10.1007/s11015-022-01289-z.

44. Yelemessov K., Baskanbayeva D., Martyushev N.V., Skeeba V.Y., Gozbenko V.E., Karlina A.I. Change in the properties of rail steels during operation and reutilization of rails. *Metals*, 2023, vol. 13, p. 1043. DOI: 10.3390/met13061043.

45. Kenjaev B., Paluanov D., Mamatkulov D., Romanova V. Methods and technologies for ensuring the reliability of excitation of synchronous generators of small hydroelectric power stations in Uzbekistan. *E3S Web of Conferences*, 2020, vol. 216, p. 01065. DOI: 10.1051/e3sconf/202021601065.

46. Solonina N., Suslov K., Solonina Z., Romanova V. Advanced approach to compensation of reactive power in isolated arctics electrical supply systems. *Journal of Physics: Conference Series*, 2021, vol. 2032 (1), p. 012113. DOI: 10.1088/1742-6596/2032/1/012113.

47. Romanova V., Khromov S., Suslov K. Multi-factor analysis of external effects influencing the operational reliability of asynchronous electric motors. *E3S Web of Conferences*, 2020, vol. 216, p. 01084. DOI: 10.1051/e3sconf/202021601084.

48. Afolalu S.A., Ikumapayi O.M., Emetere M.E., Ongbali S.O. Investigation of mechanical properties and characterization of a joint using nano flux powder for a-tig welding. *Materials Today: Proceedings*, 2021, vol. 44, pp. 2879–2883. DOI: 10.1016/j.matpr.2021.01.091.

49. Afolalu S.A., Samuel O.D., Ikumapayi O.M. Development and characterization of nano-flux welding powder from calcined coconut shell ash admixture with FeO particles. *Journal of Materials Research and Technology*, 2020, vol. 9 (4), pp. 9232–9241. DOI: 10.1016/j.jmrt.2020.06.067.

50. Karlina A.I., Kondratiev V.V., Gladkikh V., Vitkina G., Kononenko R.V. Otsenka proplavlyayushchei sposobnosti oksidnykh flyusov pri svarke A-TIG uglerodistykh i nizkolegirovannykh stalei [Evaluation of the melting ability of oxide fluxes in A-TIG welding of carbon and low-alloy steels]. *Obrabotka metallov (tekhnologiya, oborudovanie, instrumenty) = Metal Working and Material Science*, 2025, vol. 27, no. 4, pp. 96–115. DOI: 10.17212/1994-6309-2025-27.4-96-115.

Conflicts of Interest

The authors declare no conflict of interest.